Hindawi
Journal of Sensors
Volume 2021, Article ID 8859742, 10 pages
https://doi.org/10.1155/2021/8859742

*Research Article*

# Interdigital Capacitive Sensor for Cable Insulation Defect Detection: Three-Dimensional Modeling, Design, and Experimental Test

**Bing Luo,[1] Tingting Wang,[1] Fuzeng Zhang,[1] Yibin Lin,[2] Chaozhi Zheng,[2] and She Chen [2,3]**

[1]*Electrical Technology Research Institute, China Southern Power Grid, Guangzhou 510623, China*
[2]*College of Electrical & Information Engineering, Hunan University, Changsha 410082, China*
[3]*CYGE Electronic Technology (Hunan) Co. Ltd., Loudi 417000, China*

Correspondence should be addressed to She Chen; chenshe@hnu.edu.cn

Received 12 July 2020; Revised 5 January 2021; Accepted 17 March 2021; Published 31 March 2021

Academic Editor: Armando Ricciardi



Due to excellent electrical and mechanical properties, cross-linked polyethylene (XLPE) cables are widely used in power systems. Poor manufacturing techniques in the production and installation of cable joints will cause insulation defects. The interdigital capacitive (IDC) sensor has advantages of simple structure and non-contact with the center conductor and shows great potential for online monitoring on XLPE cables. This paper focuses on the 3D modeling of a fully covered IDC sensor for cable insulation detection. Firstly, a 3D finite element model of the sensor is built, and the electric field distributions are compared with those of the partially covered sensor. For the sensor with more electrode pairs, the sensitivity increases with the sensor length and tends to saturate at the length of 5 cm, while the sensitivity remains constant for the sensor with fewer electrode pairs. Then, the differences between 3D and 2D results are discussed and the sensor parameters are optimized to reduce the influence of the fringe capacitance. The simulation results indicate that air gaps between the sensor and XLPE cable are the main reason of the difference between simulation and experiment. When the electrode width is equal to the gap width, the effects of both the fringing electric field and air gaps are relatively small. Finally, several types of sensors are made and used to detect the cable joint with and without the stress cone dislocation under different excitation voltage frequency. The results show that the measured capacitance decreases with frequency and the capacitance of the cable joint with the defects is smaller than that of the normal cable joint.

## 1. Introduction

Cross-linked polyethylene (XLPE) cables are widely used for power transmission due to their excellent insulation performance [1–3]. However, due to complicated working conditions, insulation failure will occur under the long-term effect of multi-stress [4]. Besides, it is easy to cause insulation defects, for example, stress cone dislocation at the cable joint, during manual production and installation. A variety of nondestructive online methods for state monitoring and insulation detection of the XLPE cable have been put into practice. The traditional methods include partial discharge (PD) detection, tan $\delta$ measurement, sheath current monitoring, infrared camera, gas sensor, etc. There are still some limitations, such as high-frequency signal attenuation, low sensitivity, and inability to determine the aging degree of the insulation layer.

With a simple structure and non-contact with the center conductor, capacitive sensors are very suitable for characterizing the dielectric properties of insulation materials [5–8]. Several studies have been carried out on the detection of dielectric materials with capacitive sensors [9–11]. In terms of the detection principle of the IDC sensor, Mamishev et al. [12] focused on sensitivity analysis and measurement uncertainty evaluation using the stair-step parameter estimation algorithm and established the relationship between the capacitance and the dielectric constant of the sample. Sheldon and Bowler [13] developed a quasielectrostatic numerical model based on Green's function to calculate the capacitance

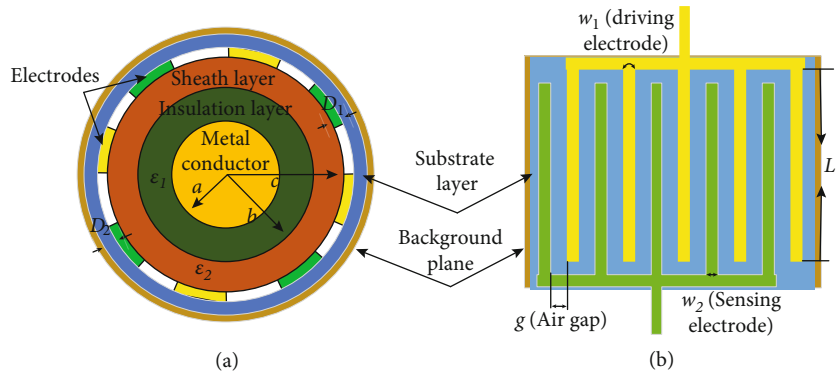


Figure 1: Fully covered interdigital capacitance sensor: (a) cross-sectional view; (b) expanded view.

Table 1: Simulation parameters of the XLPE cable.

| Conductor radius (mm) | Insulation layer | | Sheath layer | |
|---|---|---|---|---|
| | Thickness (mm) | Dielectric constant | Thickness (mm) | Dielectric constant |
| 8 | 2.5 | 2.5 | 1.9 | 5 |

of the IDC sensor and detect the insulation detection of the cable. The results show that the significant changes in the measured capacitance were the consequence of chemically induced degradation. To improve the structure of IDC sensors, Jiao et al. [14] designed a variable spacing sensor to detect the aging of dielectric materials. The simulation results show that the output capacitance and sensitivity of the sensor become greater, which is consistent with the experiment. Chen et al. [15, 16] proposed a curved IDC sensor for measuring the cable insulation. Measurements of capacitance were made on aircraft wires, and the permittivity of the insulation was obtained. The study by Glass et al. [17] indicates that the IDC sensor with a backplane has better performance in terms of capacitance, because a small air gap between the sensor and the insulation will lead to the decrease in the capacitance. The parameter optimization of IDC sensors has been performed. Liu et al. [18] improved the electric field distribution of the IDC sensor, and the results showed that the optimized sensor can detect water trees. Zhao et al. [19] focused on a partially covered IDC sensor, which is used for two-layer nuclear cables. Optimal design parameters that maximize the sensitivity of the XLPE insulation material under the cable jacket are presented. Aged cables of various types are required to be tested with custom-designed sensors. The studies of [20] mainly concentrated on optimization of electrode parameters of the IDC sensor with a 2D model. The effect of the electrode length was briefly introduced with a 3D model.

Up to now, few studies have provided detailed analysis of the parameter design by 3D simulation, and most studies have analyzed the causes of measurement errors but do not give specific measures to reduce measurement errors. In this work, a comparison of the parameter optimization is made between the 3D model and 2D model for the fully covered IDC sensor. Their effect on the output capacitance, sensitivity, and penetration depth is discussed. The relationship between the difference of optimization results and electrode parameters is studied. Then, different types of the IDC sensor are made, and the capacitances are measured for different excitation voltage frequency. Finally, the cable joint with stress cone dislocation defect is tested with the IDC sensor in the experiment.

## 2. Simulation Model and Optimization Index

*2.1. Simulation Parameters of the IDC Sensor.* Figure 1 presents the fully covered IDC sensor, which consists of an electrode layer, substrate layer, and background plane. The electrodes are divided into driving electrodes and sensing electrodes, and the number of two electrodes is equal. The driving electrode with a width of $w_1$ is applied with an excitation voltage, and the sensing electrode with a width of $w_2$ receives the response signal. The number of electrode pairs is $N$, and the thickness and length are $D_1$ and $L$, respectively. The thickness of the substrate layer is $D_2$. The dielectric constant of the insulation layer is $\varepsilon_1$, and the dielectric constant of the sheath layer is $\varepsilon_2$. The air gap between the driving electrode and the sensing electrode is $g$. $K$ is the ratio between the electrode width and the air gap width.

The backplane is connected to the ground to shield the external electromagnetic interference. Defects or aging inside the insulation layer will lead to the changes of the capacitance. By measuring this difference, the cable insulation condition can be monitored. Table 1 provides the simulation parameters of the XLPE cable (YJV1∗185).

*2.2. Comparison between the Fully Covered and Partially Covered IDC Sensors.* The IDC sensor previously designed was partially covered, which can be fixed in a clamp structure as a portable detection device. On the other hand, the fully covered IDC sensor is more suitable to be installed on the cable joint for long-term monitoring of the insulation state. Figure 2 clearly demonstrates the difference of electric field distribution of these two types of sensor. Firstly, the fully covered sensor isolates the internal electric field from the external environment, which minimizes the effect of the coupling stray electric field on the capacitance measurement. Secondly, the partially covered sensor can only measure the part of the cable insulation area covered by the sensor.

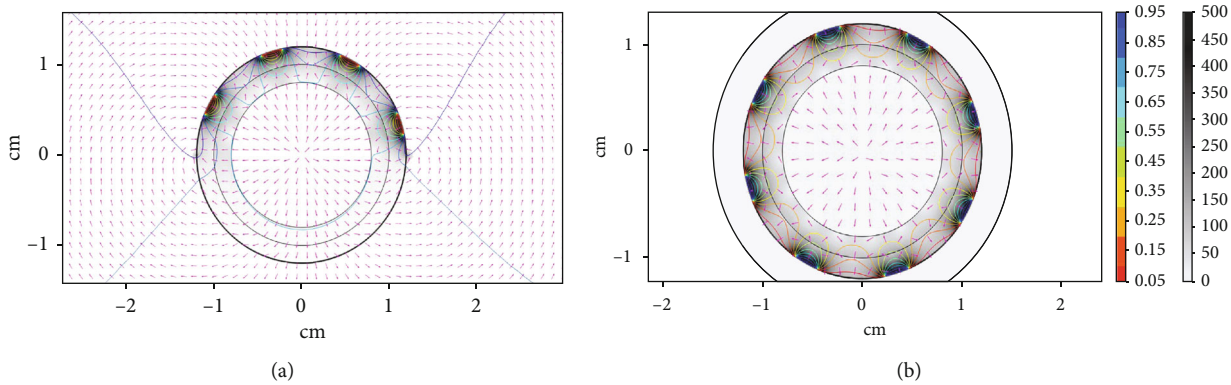


Figure 2: Electric field and potential distribution of (a) partially covered IDC sensor and (b) fully covered IDC sensor (surface electric feild: Electric field norm(V/m); arrow surface: Electric field; contour: electricity(V)).

Table 2: Sensor parameters of the 3D model.

| Thickness (cm) Background plane | Electrode layer | Substrate layer | Permittivity of substrate layer |
|---|---|---|---|
| 0.01 | 0.01 | 0.01 | 2.55 |

### 2.3. Optimization Index

*2.3.1. Output Capacitance.* The relationship between the output capacitance $C$ and sensor parameters is described by the following equation:

$$C = f(N, w_1, w_2, D_1, D_2, \varepsilon_1, \varepsilon_2, L). \quad (1)$$

Since the measured capacitance is often small, the electromagnetic interference may cause measurement error so that the variation of the capacitance is difficult to detect. Therefore, the greater the output capacitance, the higher the signal-to-noise ratio (SNR).

*2.3.2. Sensitivity.* The sensitivity $S$ of the sensor can be obtained by

$$S = \frac{\partial C}{\partial \varepsilon} = \frac{\Delta C}{\Delta \varepsilon}, \quad (2)$$

where $C$ is the output capacitance and $\varepsilon$ is the dielectric constant of the dielectric materials in the detection area. If the sensitivity is higher, the variation of output capacitance will become greater. Therefore, the small insulation defects will be detected by the IDC sensor more easily.

*2.3.3. Penetration Depth.* The penetration depth $\delta$ represents the depth of the insulation defect that the sensor can detect, which can be defined according to Reference [21]:

$$C_{a10} = 1.1 \cdot C_{a0},$$
$$\delta = b - a_{10}, \quad (3)$$

where $C_{a0}$ is the capacitance of the cable without the central conductor (the conductor radius $a$ is 0), $b$ is the outside radius of the insulation, and $a_{10}$ is the conductor radius when the capacitance $C_{a10}$ increases by 10%.

## 3. Parameter Optimization

The simulation results by the 2D model [20] show that the output capacitance increases with both $K$ and $N$, while the penetration depth decreases. Moreover, a smaller $N$ leads to a greater $K$ and a greater $S$. In our study, the sensor parameters of the 3D model are set as shown in Table 2.

*3.1. 3D Modeling and Simulation.* Ideally, the output capacitance is proportional to the electrode length $L$ and the sensitivity remains unchanged. In the 2D model, the effect of the axial electric field at the edge of the electrode is not considered, and only the radial electric field is considered. In practice, the axial fringe electric field will affect the capacitance measurement. The parameter of out-of-plane thickness in the 2D model is the same as the electrode length in the 3D model. The calculated capacitances using 2D and 3D models are shown in Figure 3. The differences in output capacitance and sensitivity between 2D and 3D simulations are quite large. With the increase in the number of electrode pairs, the difference in output capacitance increases, while the difference in sensitivity decreases. Therefore, it is necessary to use the 3D model to minimize the error when optimizing the sensor parameters.

The 3D model of the fully covered IDC sensor and XLPE cable is shown in Figure 4. The influence of the electrode length can be firstly explored. It is seen in Figure 5 that the capacitance is approximately linear with the electrode length. However, for the sensors of different electrode pairs, the variations of sensitivity with the length show different trends. When the number of electrode pairs is small, the sensitivity changes not much with the length. For a larger electrode number of 9, the sensitivity increases with the electrode length and then remains nearly unchanged when the electrode length is greater than 5 cm.

The electric field distributions along the axial and radial direction are shown in Figure 6 for the sensor with a length of 3 cm. The electric field at the edge of the sensor has a sharp increase in both the axial and radial directions. Outside the sensor, the electric field decreases with

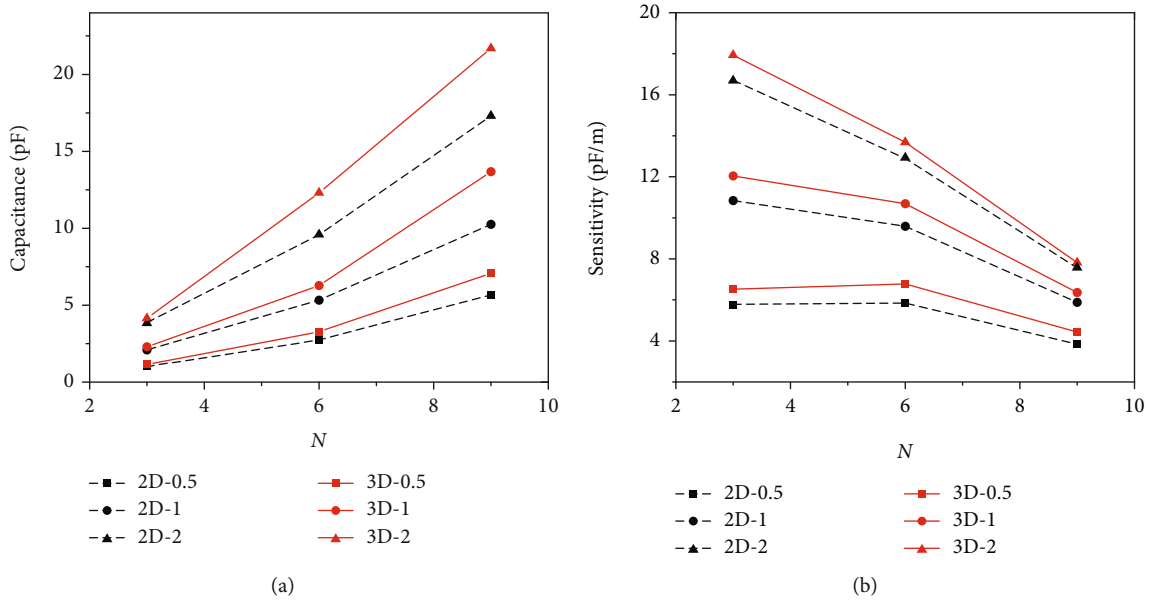


Figure 3: Comparison between 3D and 2D simulation results: (a) capacitance and (b) sensitivity. "3D-0.5" and "0.5" are the results of $K = 0.5$ in the 3D and 2D simulations, respectively.

the distance from the sensor. To investigate the influence of the fringe electric field on the insulation layer, the electric fields at the outside surface of the insulation layer in the axial direction for different electrode pairs are shown in Figure 7. It can be seen that for the sensor of $N = 3$, the electric field at the surface of the insulation layer becomes stable gradually when the cable length is at 75 cm, while for $N = 9$, the electric field still increases rapidly at this point. Therefore, the electrode length affected by the fringe electric field becomes larger with the increase in $N$.

It can be seen from Figures 6(a) and 6(b) that the electric field is large at the edge of the electrode and the electric field is concentrated on the surface of the sheath layer; that is, the penetration depth at the edge in the axial direction is affected. The overall sensitivity can be expressed as

$$\begin{aligned} S &= \frac{\partial(C_0 + \Delta C)/\partial\varepsilon}{L} \\ &= \frac{\partial[S_0 \cdot \varepsilon \cdot (L - \Delta L)]/\partial\varepsilon}{L} + \frac{\partial(\Delta C)/\partial\varepsilon}{L} \\ &= S_0 \cdot \left(1 - \frac{\Delta L}{L}\right) + \frac{(A \cdot L + B)}{L} \\ &= (S_0 + A) + \frac{(B - S_0 \cdot \Delta L)}{L}, \end{aligned} \tag{4}$$

where $S_0$ is the sensitivity which is not affected by the fringe electric field, i.e., the sensitivity in the 2D model; $C_0$ is the capacitance of the 2D model; $A$ and $B$ are the coefficients after linearization; $L$ is the length of the sensor; $\Delta C$ is the fringe capacitance; and $\Delta L$ is the length affected by the edge electric field. $\Delta C$, mainly concentrated on the surface of the sheath layer, increases with the number of electrode pairs $N$ and the width-gap ratio $K$. When the electrode pairs decrease, the sensitivity $S_0$ and the penetration depth are larger, leading to smaller $\Delta L$ and larger $A$ and $B$. Then, the 3D sensitivity does not vary with the electrode length, and the sensitivity difference between 2D and 3D models is large. However, for the sensor with more electrode pairs, the sensitivity $S_0$ and the penetration depth are small, resulting in larger $\Delta L$ and smaller $A$ and $B$. Therefore, the 3D sensitivity increases with the electrode length and the sensitivity difference becomes smaller.

*3.2. Effect of Fringe Capacitance.* It can be inferred from equation (4) that the output capacitance and the sensitivity of the 3D model are larger than those of the 2D model. For the sensor with fewer electrode pairs, the capacitances of the two models are relatively close. The capacitance difference between the two models, i.e., the fringing capacitance, increases with the number of electrode pairs and the width-gap ratio, while the sensitivity difference decreases with the increase in the number of electrode pairs. Consequently, it is necessary to weaken the fringe capacitance as much as possible.

The relationship between the fringe capacitance and the electrode parameter is presented in Figure 8. The number of electrode pairs $N$ has a greater effect than the width-gap ratio $K$. When the number of electrode pairs is small, the width-gap ratio is independent of the fringing capacitance. For $N = 6$, the role of $K$ begins to be prominent when $K$ is greater than 1. For $N = 9$, the inflection point occurs and the increase in fringe capacitance slows down when $K = 1$. Therefore, the width-gap ratio $K$ of 1 is determined, which not only guarantees a large output capacitance and sensitivity but also effectively avoids the measurement error caused by the change of fringe capacitance in practice.

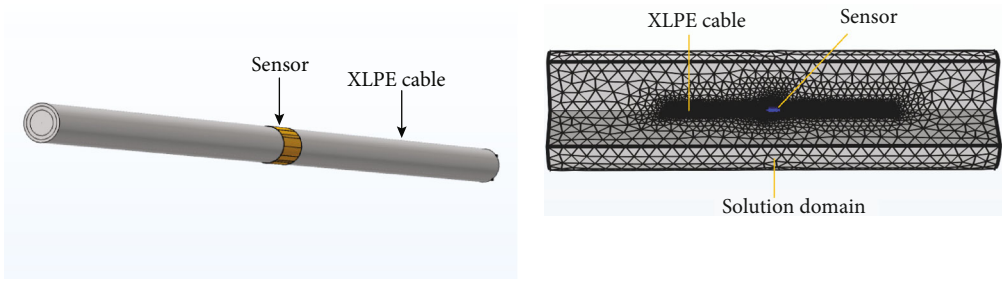


Figure 4: (a) 3D model of the sensor and XLPE cable; (b) mesh generation.

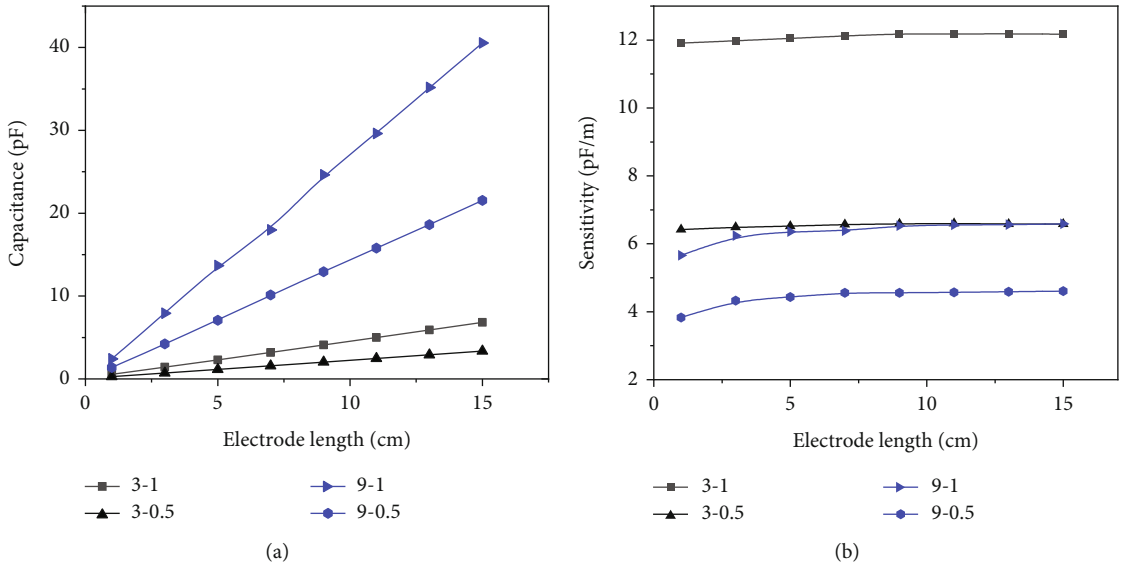


Figure 5: The effect of sensor length on (a) capacitance and (b) sensitivity (e.g., "3-1" indicates that the number of electrode pairs is 3 and the electrode width-gap ratio is 1).

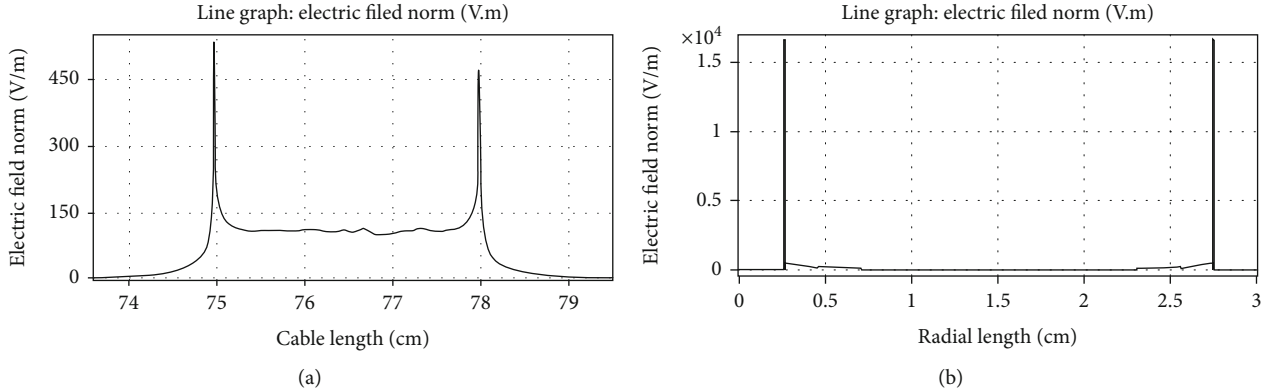


Figure 6: (a) Electric field on the surface of the sensing electrode varying with the axial length of the cable; (b) electric field varying with the radial length of the cable.

## 4. Experimental Test of the IDC Sensor

Nine sets of IDC sensors with different parameters were made. The flexible substrate layer is polyimide (PI) with a thickness of 60 $\mu$m and a dielectric constant of 4. The thickness of the copper background plane and the copper electrode is 18 $\mu$m, and the length of the sensor is 5 cm. Other parameters of the sensor are listed in Table 3.

The sensor and the experimental setup are shown in Figure 9. The YJV1∗185 cable is chosen as the sample to

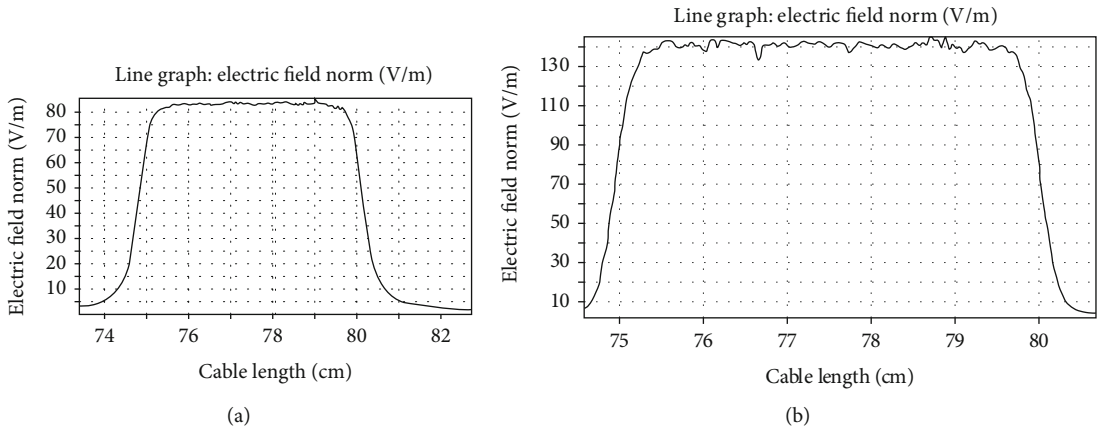


Figure 7: Electric field on the surface of the insulation layer varying with the axial length of the cable: (a) $N = 3$, $L = 5$ cm; (b) $N = 9$, $L = 5$ cm.

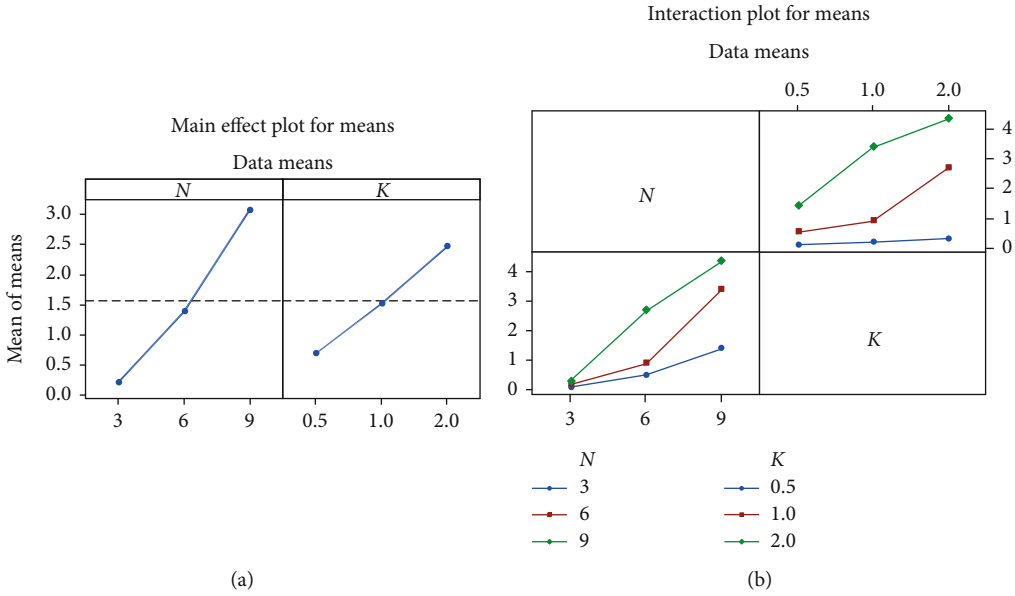


Figure 8: Effect of the number of electrode pairs $N$ and the width-gap ratio $K$ on fringe capacitance: (a) main effect; (b) interaction.

Table 3: Sensor parameters.

| Number of electrode pairs ($N$) | Width-gap ratio ($K$) | No. |
|---|---|---|
| 4 | 1/3 | 1 |
| | 1 | 2 |
| | 3 | 3 |
| 6 | 1/4 | 4 |
| | 1 | 5 |
| | 4 | 6 |
| 9 | 1/2 | 7 |
| | 1 | 8 |
| | 2 | 9 |

be tested. The conductor radius is 0.8 cm, the thickness of the insulation layer is 0.2 cm, and the thickness of the sheath layer is 0.19 cm. Impedance analyzer E4990A and clamp 16089A are used to measure the cable insulation capacitance.

*4.1. Comparison of the Measured and Simulated Capacitance.* The measured capacitance of the normal cable is illustrated in Figure 10. The measured capacitance increases with the number of electrode pairs and the width-gap ratio, which is consistent with the simulation result. Furthermore, the measured capacitance gradually decreases with the excitation voltage frequency, and the measured capacitance and the measurement error increase with the number of electrode pairs and the width-gap ratio.

In the simulation, the dielectric constant of cable insulation is specified, so the calculated capacitance is independent of frequency. In order to compare the experimental capacitance with simulated values, the excitation voltage frequency corresponding to the theoretical calculation should be determined. According to the previous section, the fringe capacitance is in positive correlation with the number of electrode

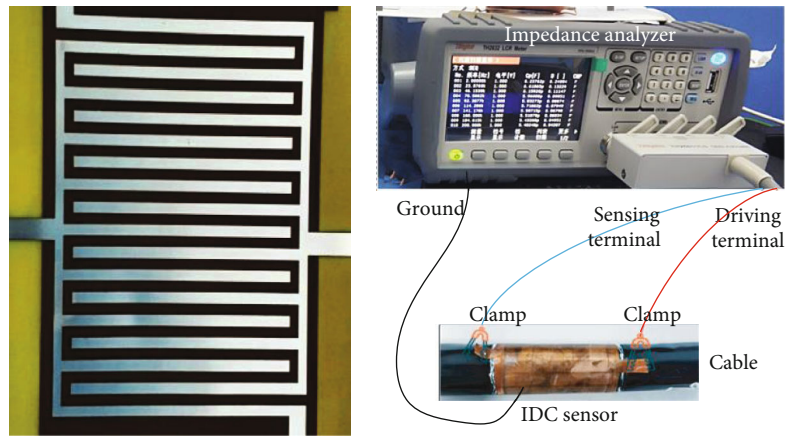


Figure 9: (a) IDC sensor and (b) schematic diagram of the experimental setup.

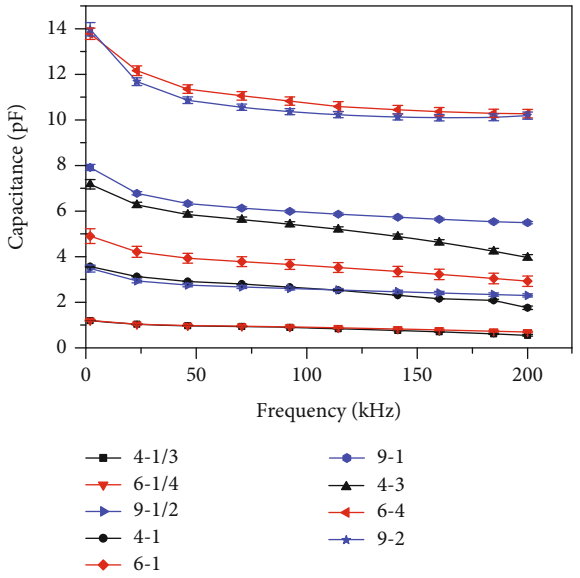


Figure 10: Variations of the measured capacitance of the XLPE cable sample with frequency (e.g., "4-1/3" is the sensor with 4 pairs of electrodes and the width-gap ratio of 1/3).

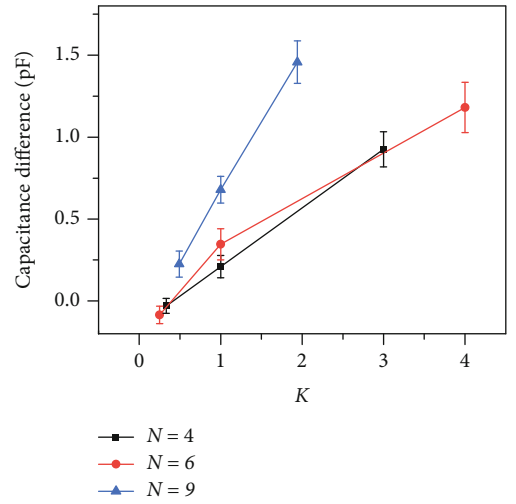


Figure 11: Capacitance difference between simulation and experiment (e.g., "4" is the sensor with 4 pairs of electrodes).

pairs and the width-gap ratio. At the reference frequency of around 180 kHz, the measured capacitance is similar to the simulated capacitance of the no. 1 sensor.

The simulation results are compared with the experimental results, and their differences are provided in Figure 11. With the increase in the electrode width-gap ratio $K$, the measurement error increases; that is, the influence of the environmental interference rises. When $K$ is greater than 1, the error is relatively large. When the tightness degree between the sensor and the cable surface changes due to vibration or other reasons, the air gap capacitance will have little effect on the sensor ($K < 1$).

When $N$ is 6 and $K$ is 1/4, the measured capacitance is larger than the simulated value and the fringing capacitance of the sensor is larger than that of the sensor ($N$ is 4 and $K$ is 1/3), which is consistent with the previous results. Interestingly, this is contrary to the measurement result of other sensors. The comparison results for other sensors indicate that the simulation value is larger than the experimental value with the increase in $K$ and $N$. One main reason for that is the fact that the electrodes cannot completely fit onto the cable surface, resulting in air gaps between the sensor and the cable surface. The larger the width-gap ratio, the wider the electrode and the weaker the ability to fit the surface. Besides, the electric field is stronger near the cable surface, resulting in the difference between the measured capacitance and the theoretical value.

*4.2. Detection of Stress Cone Dislocation Defect.* The shielding layer needs to be stripped off to make the cable joint. The electric field concentrating at the fracture may cause the breakdown of cables. The stress cone is usually used to improve the electric field distribution. The dislocation of the stress cone from the shielding layer is one of these typical

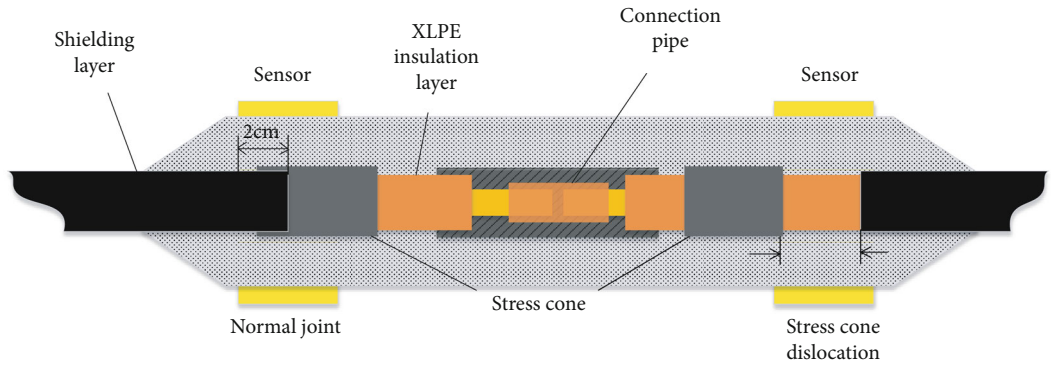


Figure 12: Schematic diagram of the stress cone dislocation and normal cable joint.

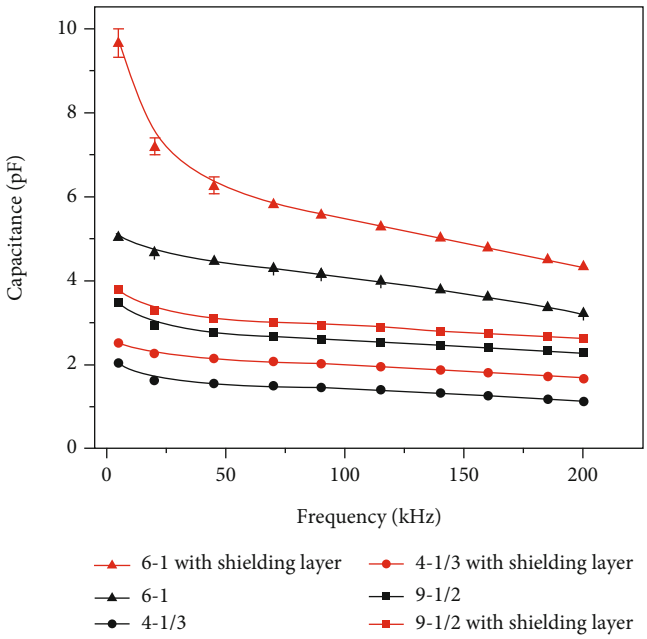


Figure 13: Detection of stress cone dislocation: "6-1" means the defective cable without the shielding layer and "6-1 with shielding layer" is the normal cable with the shielding layer.

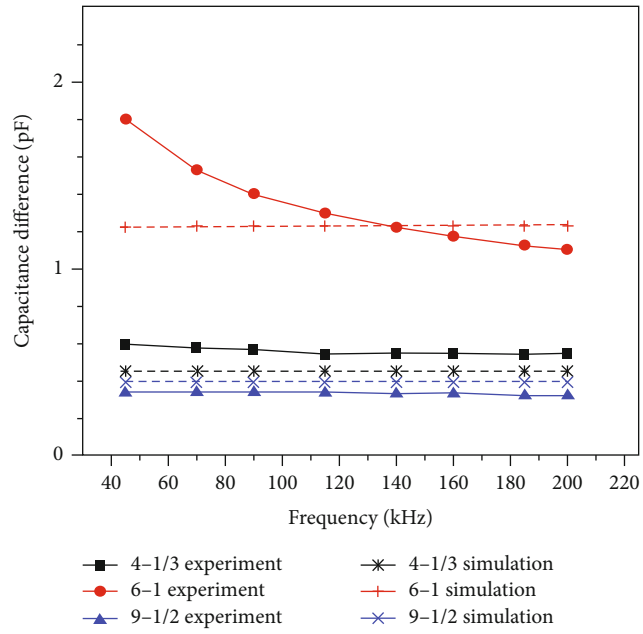


Figure 14: Measured capacitance difference and simulated capacitance difference between the normal and defective cable joints: "6-1 experiment" means the measured capacitance difference of the "6-1" sensor and "6-1 simulation" means the simulated capacitance difference of the "6-1" sensor.

Table 4: The simulated capacitance in the defective and normal cable joint.

| Number | Defective cable joint (pF) | Normal cable joint (pF) | Capacitance difference (pF) |
|---|---|---|---|
| 1 | 0.6018 | 1.0532 | 0.4514 |
| 5 | 3.4433 | 4.674 | 1.2307 |
| 7 | 2.9289 | 3.3223 | 0.3934 |

defects. The IDC sensors will be used to detect the defect in the experiment. The cables are divided into two groups, one group of the normal cable joint and the other group of the cable joint with stress cone dislocation, which is shown in Figure 12. For the normal cable joint, the shielding layer about 2 cm long is wrapped on the surface of the insulation layer, while for the defected cable joint, the shielding layer is not. The output capacitance of the cable joint with and without the shielding layer is plotted in Figure 13. It is found that the measured capacitances of the cable joints with and without the shielding layer are quite different. The capacitance difference between the normal and defective cable joints varies greatly with the electrode parameters and little with the frequency.

The simulated capacitance and the capacitance variation between the normal and defective cable joints are listed in Table 4. The sheath layer of the cable is peeled off and reattached on the insulation layer, so the measured capacitance should be smaller than the actual value. It is seen in Figure 14 that the trend of capacitance difference is similar to the experiment. At 45-200 kHz, the capacitance difference of the "9-1/2" sensors and "4-1/3" sensors between the simulation and experiment is less than 0.1 pF

and 0.2 pF. At 70-200 kHz, the capacitance difference between the simulation and experiment of the "6-1" sensor is less than 0.3 pF. Especially, at the frequency of around 140 kHz, the capacitance difference of "4-1/3" sensors, "6-1" sensor, and "9-1/2" sensors is 0.099 pF, 0.007 pF, and 0.061 pF, respectively.

The capacitance variation of the sensors of no. 5, no. 1, and no. 7 declines in sequence. If the stress cone dislocation occurs at the cable joint, the measured capacitance should be much smaller than the normal one, and the IDC sensor can detect the defect effectively. Moreover, provided that the penetration depth of the IDC sensor reaches the insulation layer, the greater sensitivity leads to the larger measured capacitance variation. The penetration depth that has already reached the insulation layer and the sensitivity of the no. 5 sensor are, respectively, smaller and larger than those of the no. 1 sensor, leading to the larger capacitance variation. Compared with the no. 1 sensor, the no. 5 sensor has a smaller penetration depth that has reached the insulating layer and higher sensitivity, which leads to a larger capacitance change. The no. 7 sensor has a smaller penetration depth and similar sensitivity with the no. 1 sensor, so the capacitance changes even less. Therefore, the measured capacitance by the no. 5 sensor has the largest difference, which makes it easier to distinguish between the normal cable joint and cable joint with stress cone dislocation.

## 5. Conclusions

This paper is aimed at studying a fully covered IDC sensor for the insulation defect detection of the XLPE cable. The 3D simulation results are compared with the 2D results to optimize the electrode parameters. Furthermore, the IDC sensors are used to test the normal and defective cable joints in the experiment. The following is a summary of conclusions.

(1) The output capacitance is proportional to the electrode length. For the IDC sensor with more electrode pairs, the sensitivity is independent of the electrode length, while the sensitivity initially increases and tends to be stable, for the sensor with fewer electrode pairs. The recommended length of the electrode is larger than 5 cm

(2) The fringing capacitance is the reason for the difference between the 3D and 2D results. The electric field at the edge of the sensor is large, leading to the weakened penetration ability. The capacitance difference increases with the electrode pairs while the sensitivity shows a declined trend. The recommended value of the width-gap ratio is 1 so as to reduce the fringing capacitance

(3) The measured capacitance decreases with the increasing frequency. The greater the electrode pairs and the width-gap ratio are, the larger the measured capacitance is. When the width-gap ratio is 1, the capacitance difference between the simulation and experiment is relatively small; i.e., the air gap capacitance has little influence

(4) In the stress cone dislocation detection experiment, the capacitance of the defective cable is smaller than that of the normal cable. The capacitance difference between the simulation and experiment at a frequency of 140 kHz is small (less than 0.1 pF). It is shown that the greater sensitivity leads to the larger measured capacitance variation

## Data Availability

The data of the electric field distribution and the measured capacitance, used to support the findings of this study, is supplied by B. Luo and T. T. Wang under license and so cannot be made freely available. Requests for access to these data should be made to S. Chen (chenshe@hnu.edu.cn).

## Conflicts of Interest

The authors declare that there is no conflict of interest regarding the publication of this paper.

## Acknowledgments

This research was funded by the Open Project Fund of National Engineering Laboratory for Ultra High Voltage Engineering Technology (Kunming and Guangzhou) under Grant NEL201804 and "Huxiang Young Talents Plan" Project of Hunan Province (2019RS2066).

## References

[1] H. Orton, "History of underground power cables," *IEEE Electrical Insulation Magazine*, vol. 29, no. 4, pp. 52–57, 2013.

[2] U. Schichler, "A sensitive method for on-site partial discharge detection on XLPE cable joints," in *Proceedings of 5th International Conference on Properties and Applications of Dielectric Materials*, pp. 1099–1102, Seoul, South Korea, May 1997.

[3] S. Tenbohlen, D. Denissov, S. M. Hoek, and S. M. Markalous, "Partial discharge measurement in the ultra high frequency (UHF) range," *IEEE Transactions on Dielectrics and Electrical Insulation*, vol. 15, no. 6, pp. 1544–1552, 2008.

[4] E. Gulski, J. J. Smit, P. Seitz, and J. C. Smit, "PD measurements on-site using oscillating wave test system," in *Conference Record of the 1998 IEEE International Symposium on Electrical Insulation (Cat. No.98CH36239)*, pp. 420–423, Arlington, VA, USA, June 1998.

[5] M. C. Zaretsky, L. Mouayad, and J. R. Melcher, "Continuum properties from interdigital electrode dielectrometry," *IEEE Transactions on Electrical Insulation*, vol. 23, no. 6, pp. 897–917, 1988.

[6] H.-K. Lee, S.-I. Chang, and E. Yoon, "A capacitive proximity sensor in dual implementation with tactile imaging capability on a single flexible platform for robot assistant applications," in *19th IEEE International Conference on Micro Electro Mechanical Systems*, pp. 606–609, Istanbul, Turkey, January 2006.

[7] R. T. Sheldon, "Electrical and capacitive methods for detecting degradation in wire insulation," Ph.D. dissertation, Elect. Eng. Iowa State Univ., Ames, IA, USA, 2012.

[8] A. V. Mamishev, Y. Du, B. C. Lesieutre, and M. Zahn, "Development and applications of fringing electric field dielectrometry sensors and parameter estimation algorithms," *Journal of Electrostatics*, vol. 46, no. 2-3, pp. 109–123, 1999.

[9] R. H. Bhuiyan, R. A. Dougal, and M. Ali, "Proximity coupled interdigitated sensors to detect insulation damage in power system cables," *IEEE Sensors Journal*, vol. 7, no. 12, pp. 1589–1596, 2007.

[10] A. A. Nassr, W. H. Ahmed, and W. W. El-Dakhakhni, "Coplanar capacitance sensors for detecting water intrusion in composite structures," *Measurement Science and Technology*, vol. 19, no. 7, article 75702, 2008.

[11] A. A. Nassr and W. W. Eldakhakhni, "Damage detection of FRP-strengthened concrete structures using capacitance measurements," *Journal of Composites for Construction*, vol. 13, no. 6, pp. 486–497, 2009.

[12] A. V. Mamishev, S. R. Cantrell, Y. Du, B. C. Lesieutre, and M. Zahn, "Uncertainty in multiple penetration depth fringing electric field sensor measurements," *IEEE Transactions on Instrumentation & Measurement*, vol. 51, no. 6, pp. 1192–1199, 2002.

[13] R. T. Sheldon and N. Bowler, "An interdigital capacitive sensor for nondestructive evaluation of wire insulation," *IEEE Sensors Journal*, vol. 14, no. 4, pp. 961–970, 2014.

[14] J. Jiao, L. Li, B. Wu, and C. He, "Novel capacitive proximity sensors for assessing the aging of composite insulators," *Sensors and Actuators A: Physical*, vol. 253, pp. 75–84, 2017.

[15] T. Chen, J. R. Bowler, and N. Bowler, "Analytical solution for capacitance calculation of a curved patch capacitor that conforms to the curvature of a homogeneous cylindrical dielectric rod," *Applied Physics Letters*, vol. 104, no. 3, article 032901, 2014.

[16] T. Chen and N. Bowler, "Analysis of a capacitive sensor for the evaluation of circular cylinders with a conductive core," *Measurement Science and Technology*, vol. 23, no. 4, article 045102, 2012.

[17] S. W. Glass, M. N. Al-Imran, L. S. Fifield, and M. Ali, "Simulation and experimental results of interdigital capacitor (IDC) sensors to monitor insulation degradation of cables," in *2019 IEEE Conference on Electrical Insulation and Dielectric Phenomena (CEIDP)*, pp. 368–372, Richland, WA, USA, October 2019.

[18] Y. Liu, Y. Huang, R. Tang, and B. Wang, "Application of interdigital capacitive sensors for detecting power cable insulation damage," in *2015 IEEE International Conference on Mechatronics and Automation (ICMA)*, pp. 1795–1799, Beijing, China, August 2015.

[19] Z. H. Shao and N. Bowler, "Capacitive nondestructive evaluation of aged cross-linked polyethylene (XLPE) cable insulation material," in *Proceedings of the 18th International Conference on Environmental Degradation of Materials in Nuclear Power Systems–Water Reactors*, pp. 1303–1313, Portland, OR, USA, August 2017.

[20] C. Zheng, S. Chen, F. Zhang, Y. Xu, S. Chen, and T. Wang, "Three-dimensional modeling and optimization of a fully-covered interdigital capacitive sensor for power cable insulation detection," in *2019 IEEE 3rd International Electrical and Energy Conference (CIEEC)*, pp. 1485–1490, Beijing, China, September 2019.

[21] T. Chen, *Capacitive sensors for measuring complex permittivity of planar and cylindrical structures*, Ph.D. dissertation, Elect. Eng. Iowa State Univ., Ames, IA, USA, 2012.